Contact-area dependence of frictional forces: Moving adsorbed antimony nanoparticles

Claudia Ritter,* Markus Heyde,† Bert Stegemann,‡ and Klaus Rademann

Institute of Chemistry, Humboldt Universität zu Berlin, Brook-Taylor-Strasse 2, D-12489 Berlin, Germany

Udo D. Schwarz

Department of Mechanical Engineering, Yale University, P. O. Box 208284, New Haven, Connecticut 06520-8284, USA

Antimony nanoparticles grown on highly oriented pyrolytic graphite and molybdenum disulfide were used as a model system to investigate the contact-area dependence of frictional forces. This system allows one to accurately determine both the interface structure and the effective contact area. Controlled translation of the antimony nanoparticles (areas between 10 000 and 110 000 nm^2) was induced by the action of the oscillating tip in a dynamic force microscope. During manipulation, the power dissipated due to tip-sample interactions was recorded. We found that the threshold value of the power dissipation needed for translation depends linearly on the contact area between the antimony particles and the substrate. Assuming a linear relationship between dissipated power and frictional forces implies a direct proportionality between friction and contact area. Particles about 10 000 nm^2 in size, however, were found to show dissipation close to zero. To explain the observed behavior, we suggest that structural lubricity might be the reason for the low dissipation in the small particles, while elastic multistabilities might dominate energy dissipation in the larger particles.

I. INTRODUCTION

In the ongoing endeavor to miniaturize devices, there is currently a tradeoff between reliability and degree of miniaturization for devices featuring sliding components, as in, e.g., microelectromechanical systems.[1] This is because friction and wear appear to play an increasingly important role in nanoscale machines due to the breakdown of conventional lubrication schemes and the higher percentage of surface atoms, which cause surface forces to become relatively important for the overall system behavior. As a consequence, the contact-area dependence of frictional forces in the nanometer regime has become a topic of considerable interest.

Most nanoscopic attempts to shed light on this issue have been performed by studying the frictional force F_f as a function of the externally applied loading force F_l using friction force microscopy (see, e.g., Refs. 2–15). Predominantly, F_f has been found to be a strongly nonlinear function of F_l, in contrast to the macroscopic behavior described by Amontons' law $F_f = \mu F_l$, where the constant factor μ represents the so-called friction coefficient. A frequently used approach to explain the nonlinear behavior and to simultaneously obtain information about the contact-area dependence of the frictional forces is to introduce the shear stress τ

$$\tau = F_f / A_{\text{contact}}, \tag{1}$$

where A_{contact} is the actual contact area. Using various contact mechanical models to calculate A_{contact} as a function of F_f (all essentially derivatives of the Hertzian contact model), it has been found that $\tau = $ const or, in other words, that $F_f \propto A_{\text{contact}}$.[5–9,12] In order to explain this observation, Wenning and Müser[16] used an earlier result[17] suggesting that $F_f \propto F_l A_{\text{contact}}^{-1/2}$ for dry, amorphous, flat surfaces. Assuming that the structure of the tip apex is amorphous and that the contact shows Hertzian or at least quasi-Hertzian behavior under load with $F_l \propto A_{\text{contact}}^{3/2}$, it then follows $F_f \propto A_{\text{contact}}$. Thus,

within this theory, the $F_f \propto A_{\text{contact}}$ dependence is essentially a consequence of the specific mechanical deformation behavior of the contact and not a general property of surfaces.

On a more fundamental level, the question regarding the contact-area dependence of friction is related to the occurrence of so-called structural lubricity,[18] which was originally termed "superlubricity."[19] This phenomenon basically describes the reduction of the shear stresses on atomically flat surfaces with increasing size due to a reduction of the potential barrier between stable states caused by lattice mismatch, as is evidenced by a growing number of theoretical[17–21] and experimental[22–25] studies. Structural lubricity is expected to lead to very low shear stresses between disordered or incommensurate atomically flat surfaces once the contact areas have reached a certain size.[18] This, however, holds only as long as the interbulk stiffness is high enough to ensure that the two bodies move essentially as rigid bodies.[18] Otherwise, energy might be dissipated due to considerable internal elastic deformations of the sliding objects, i.e., elastic jumps between different mechanically stable or metastable configurations. Such processes are often referred to as elastic multistabilities.

The above discussion highlights the importance of understanding how friction depends on the contact area at the nanometer scale independent of implications whether or not specific contact mechanical models are applicable, or what the exact geometry of the contact looks like. However, studies addressing this issue have not been published so far due to a lack of adequate experimental approaches. Here, we present measurements of the power dissipation occurring during the controlled movement of nanometer-sized antimony particles on highly oriented pyrolytic graphite (HOPG) and molybdenum disulfide (MoS$_2$), respectively, as a function of the particle size. The results will then be related to the frictional properties of the interface. Due to the unique approach, which involves the use of a scanning force microscope driven in the dynamic mode, the experiments are not

affected by any assumptions of the elastic behavior of the contact under load.

II. EXPERIMENTAL

A. Sample preparation

The samples were prepared in an ultrahigh-vacuum chamber with a base pressure of less than 6×10^{-10} mbar. Antimony was deposited by thermal evaporation of the solid material and condensation of the vapor onto the freshly cleaved (0001) surfaces of HOPG and MoS_2 kept at room temperature. The deposition rate and thus the effective layer thickness were calibrated with a water-cooled crystal microbalance. Nanometer-sized particles were spontaneously formed by diffusion and aggregation of the deposited material on the surfaces. The HOPG and MoS_2 samples were produced under identical preparation conditions to obtain like morphologies on both substrate surfaces.

B. Experimental setup

The manipulation experiments were performed under ambient conditions using a home-built scanning force microscope (SFM) in conjunction with a specially developed software.[26] A commercially available cantilever (Pointprobe NCL) with resonant frequency $\omega_0/2\pi = 172.94$ kHz, quality factor $Q_{cant} = 546.8$, and spring constant $k = 45$ N/m was used to operate the SFM under ambient conditions in the dynamic mode (tapping mode with constant oscillation amplitude) during the experiments on HOPG. The cantilever chosen for the experiments on MoS_2 featured $\omega_0/2\pi = 172.00$ kHz, $Q_{cant} = 554.8$, and $k = 46$ N/m. The value of the spring constant k was calculated using the individually measured thickness, width, and length of each cantilever as provided by the manufacturer, and shows an estimated error of $\pm 20\%$.

The instrument[26] and its later modifications[27] have been described elsewhere. In short, the characteristic features of the instrument that distinguish it from other setups are (a) the use of hardware-linearized piezo elements, (b) a separation of the lateral xy and vertical z motion, and (c) the manipulation interface of the software. The hardware-linearized scan motion of the piezo elements, realized by integrated capacitive displacement sensors, suppresses nonlinearities and hysteresis to values lower than 0.03% and features a repositioning accuracy of better than 2 nm, i.e., less than 0.001% of our maximum scan range of 240×240 μm^2. The high precision enables the exact positioning of the tip at chosen locations during the manipulation experiments. The separation of lateral xy and vertical z motion allows a hardware compensation of the sample tilt and thus a more precise operation of the feedback loop due to higher possible gains (see Ref. 27 for more details). Finally, the manipulation interface of the software offers convenient control of all manipulation steps by mouse clicks. The interface was written in Borland DELPHI (Borland Inprise Corporation, Scotts Valley, CA) for Object Windows and enables fast switching between imaging in a raster scan mode and the manipulation mode and back again. Switching between these modes does not entail any scanner movement; the position of the tip with respect to the sample surface is accurately retained.

C. Experimental procedure to determine the threshold power to move an individual particle

All manipulation experiments were performed in the so-called dynamic surface modification (DSM) mode, which has been introduced in Ref. 27. This manipulation technique is based on incrementing the power input into the sample surface by the oscillating tip in the dynamic SFM mode. The particles can be translated when the power input exceeds a threshold value necessary to overcome the friction force of the adsorbed particle. By changing the amplitude of the dither piezo A_{dither} that drives the cantilever oscillations while the feedback loop is continuously working, it is possible to switch between an imaging mode and a manipulation mode with variable power input into the sample. Thus, an individual adaptation to the sample properties is feasible.

In the case of a free cantilever, increasing the amplitude of the dither piezo A_{dither} leads to an increase of the effective oscillation amplitude, which scales linearly with the excitation. During the manipulation experiments, however, the excitation is increased when the cantilever is still in feedback. The feedback system tries to maintain the preselected setpoint amplitude of the cantilever A_{set} by decreasing the distance between cantilever and sample. Recording A_{dither}, A_{set}, and the phase angle φ (which represents the difference between driving frequency and cantilever response) allows one to calculate the power dissipation during the manipulation, as discussed below.

For this calculation we use the method introduced by Anczykowski *et al.* in Ref. 28. In short, the analysis starts from the fact that for a dynamic system in steady-state equilibrium, the average power input P_{in} that is fed into the cantilever by the dither piezo must equal the average power dissipated by the motion of the cantilever P_0 and by tip-sample interaction P_{tip}:

$$P_{in} = P_0 + P_{tip}. \tag{2}$$

To determine the input power P_{in}, it is assumed that (i) the cantilever possesses a spring constant k and is driven sinusoidally at the frequency ω, which results in a sinusoidal steady-state response, and (ii) intrinsic damping of the cantilever as well as damping by the surrounding medium (in our case air) can be considered by a single overall damping constant. Condition (ii) can be shown to hold as long as $A_{set} \gg A_{dither}$, which is usually very well satisfied.[28] If additionally, to simplify the result, the driving frequency ω is chosen to be identical with the eigenfrequency of the free cantilever ω_0, which was the case during our measurements, the power dissipated by the tip-sample interaction P_{tip} can be obtained from

$$P_{tip} = \frac{1}{2} \frac{k\omega_0}{Q_{cant}} [Q_{cant} A_{dither} A_{set} \sin \varphi - A_{set}^2]. \tag{3}$$

Note that no assumptions have been made concerning the nature of the tip-sample interaction, except that the motion of the cantilever stays sinusoidal to a good approximation. We

verified the validity of this condition by analysis of the fast Fourier transformation (FFT) spectra of the cantilever oscillations for the cases of the free cantilever and the cantilever in feedback. We also varied the excitation amplitude of the cantilever to check the FFT spectra for different values of energy dissipation. The tested parameter range is the same as that necessary for the experiments in which particles are translated. We found an increasing ratio of the higher harmonic oscillations for the change from free cantilever to cantilever in feedback, which further increased with increasing excitation amplitude. However, even during strong tip-sample interaction, the ratio of the higher harmonics to the resonant frequency is only about 1%. Thus, the calculation of the dissipated power according to Eq. (3) should be readily applicable to our manipulation experiments.

Before we leave the subject, let us note that translation of particles can also be achieved by operating the SFM in contact mode (see, e.g., Refs. 29–31). The difficulty with this approach, however, is that it is not that trivial to find a suitable cantilever which on the one hand allows one to image without pushing nanoparticles around while low loading forces are applied, and on the other hand enables one to exert enough pressure at high loading forces to manipulate even large particles. This is much more readily achieved in dynamic mode, where the excitation amplitude can be adjusted over orders of magnitude, if necessary, to switch between gentle imaging and manipulation of even the biggest particles.

III. RESULTS

In this section, we will first characterize our experimental system. Subsequently, we will demonstrate our ability to perform controlled nanomanipulation experiments using the DSM technique by two examples. Finally, we will describe the experiments to evaluate the relationship between power dissipation and contact area of the translated particle, i.e., to find the threshold value necessary to move a particle, in the third part.

A. Sample characterization: Morphology and structure of the nanoparticles

The samples were characterized by SFM and transmission electron microscopy (TEM). As described earlier, self-organized growth on the HOPG (0001) surface at room temperature lead to the formation of flower-shaped, ramified nanoparticles.[32] As demonstrated in Fig. 1, the shape and the size distribution of the nanoparticles obtained on MoS_2 (0001) are comparable to those on HOPG (0001) when the same deposition parameters (deposition rate 0.1 Å/s, effective layer thickness 10 monolayers for the images shown) are applied. The dimensions of the nanoparticles were determined from SFM and TEM data. The lateral diameter is typically about 120–400 nm and the height ranges from 20 to 35 nm.

Additionally, information about the crystalline character of the antimony particles on both substrates was obtained by TEM. The insets in Fig. 1 reveal dark contour lines inside the
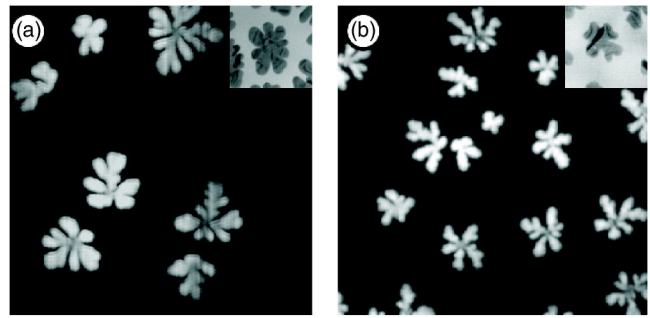
FIG. 1. SFM (2.5×2.5 μm^2) and TEM (0.66×0.66 μm^2) images of the two sample surfaces (a) Sb on HOPG and (b) Sb on MoS_2. The insets show bright field TEM images of typical flower-shaped Sb particles on each surface. The dark contour lines inside the particles are bending contours produced by the strained crystalline particles.

particles. In an accompanying study, these patterns were identified as bending contours, indicating a strained crystalline structure.[32] Therefore, we conclude that the particles consist of various crystalline areas of varying relative orientation and areas of enhanced stress.

B. Controlled nanomanipulation by the DSM technique

The particle translations presented in this article were performed using the DSM technique introduced in Sec. II C. To start, a SFM image is taken using a nonmodifying value for the cantilever driving amplitude A_{dither} in order to obtain an overview of the area of interest. Subsequently, the software is switched to the manipulation mode, which allows the tip to be positioned at a desired location near the particle to be manipulated. Next, the value of A_{dither} is increased and the tip is moved (seemingly) across the particle along a chosen path. Finally, the same area is imaged again with the same nonmodifying value of A_{dither} used for the initial image to check the result of the attempted manipulation experiment. If A_{dither} was large enough, the particle moved; otherwise, it remained stuck at the original position. Figure 2 illustrates this procedure. Two antimony particles are labeled (*a* and *b*) for convenient observation of their movements. The white arrows indicate the trajectory of the manipulating tip, while the gray arrows show the resulting motion of the particle. The dotted arrows mark the path of the tip during the preceding step.

Such manipulation experiments can be repeated several times with reproducible results and without destroying or modifying the antimony nanoparticles. As illustrated in Fig. 2, the resulting motion of the manipulated particle generally consists of a combination of translation and in-plane rotation, depending on the selected contact point and the trajectory of the manipulating tip. To achieve primarily a translation of the particle, the trajectory of the manipulating tip has to be in line with the center of gravity of the desired particle [see Figs. 2(c) and 2(d)]. A nanostructure consisting of about 50 antimony nanoparticles was built up as illustrated in Fig. 3 in order to demonstrate that the DSM technique enables us to arbitrarily translate particles in a controlled way: The letters "H" and "U" (for Humboldt University) were formed from randomly distributed nanoparticles.
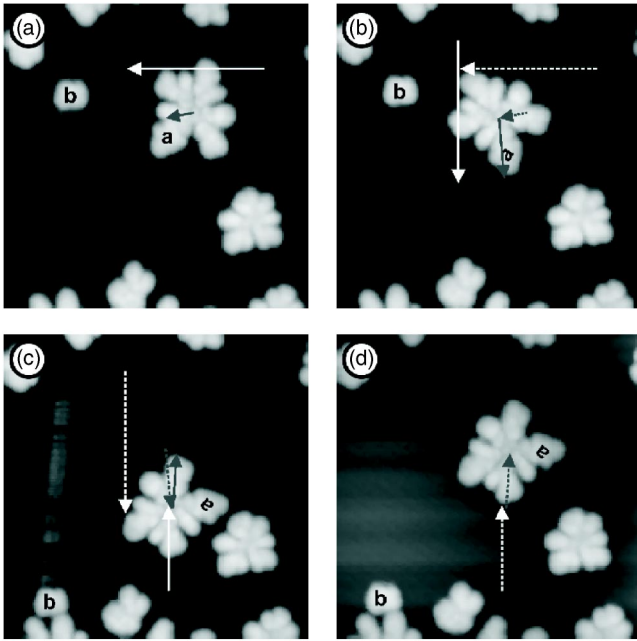
FIG. 2. Illustration of the manipulation procedure (SFM images, Sb on HOPG, image size 1×1 μm^2, height of particle a is 26 nm). (a) Overview of the particle of interest (labeled with a) and the surrounding area. A white and a gray arrow indicate the path of the subsequent tip motion and the resulting dislocation of the particle, respectively. (b) Topography after the manipulation. Comparison with (a) shows that the particle a experienced a lateral translation of 83 nm and an in-plane rotation of 58°. For the next manipulation step, another contact point between the particle and the tip was selected, visualized again by a white arrow. (c) Result of the second manipulation step, revealing a translation of 211 nm and an in-plane rotation of 77°. (d) Final result after the third manipulation step. This time, the translational motion of 175 nm was accompanied only by a small in-plane rotation of about 3°. In (c) it is visible that particle b was accidentally translated during the imaging process. The contact area of this particle is slightly below 10 000 nm^2 and thus in the range of very low power dissipation. In contrast, power dissipation during the manipulation of particle a with a contact area of about 62 000 nm^2 is much higher, and stable imaging is easily achieved.

C. Determination of the threshold power to move a particle as a function of the contact area

Similar experiments as those illustrated in Fig. 2 were performed to determine the threshold power of the excitation amplitude that is necessary to translate an antimony particle with a specific contact area. The manipulating tip was moved repeatedly across the desired particle while continuously increasing the excitation amplitude from attempt to attempt until the particle moved. During the manipulation, the excitation amplitude A_{dither}, the set-point amplitude A_{set}, and phase shift φ were recorded simultaneously. With these values, the threshold power P_{tip} was calculated using Eq. (3). All manipulation experiments were performed in the same manner in order to obtain comparable results. Specifically, the tip was always moved at the same velocity (2μm/s) in the x direction across the particle. Maintaining the same direction of motion is crucial to reduce effects due to the asym-
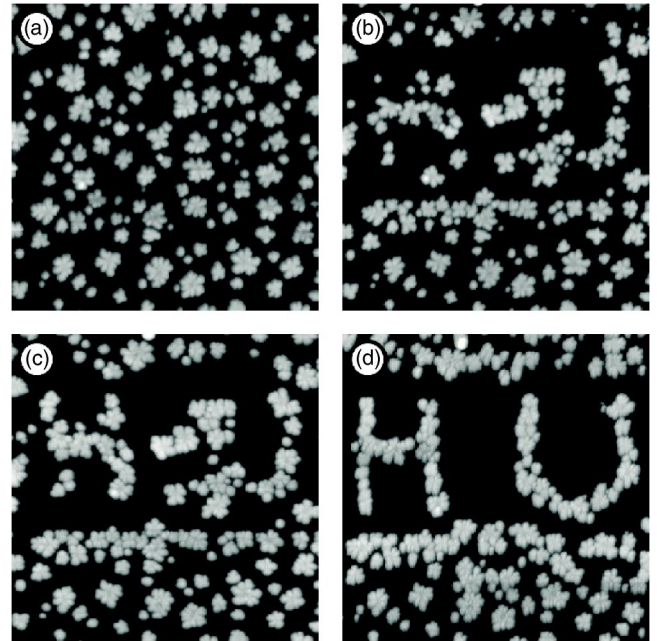
FIG. 3. Formation of the letters "H" and "U" (for Humboldt University) as an example for an intentionally composed two-dimensional nanostructure. (a)–(c) illustrate different steps of the assembly process, (d) the final result. The final structure consists of 50 Sb nanoparticles; the substrate is HOPG. The average particle height is about 30 nm, and the size of all images is 4×4 μm^2.

metric tip shape (cf. Sec. IV, where we discuss how the tip angle influences the lateral component of the tip-particle coupling). Therefore, we are not able to draw any conclusions on the dependence of the frictional forces on the sliding direction relative to the substrate lattice. The point of impact of the tip at the particle was chosen such that the particle did not rotate during manipulation to avoid complications in the data interpretation caused by an eventual rotation. Finally, we emphasize that all manipulation experiments were carried out on atomically flat, defect-free terraces to prevent surface steps from influencing our data.

The experiments are analyzed as a function of the particle size A_{particle}, which is equal to the actual contact area between particle and substrate. The results for both substrates, HOPG (23 data points, reflected by triangles) and MoS$_2$ (12 data points, circles), are shown in Fig. 4. The contact areas of the various particles range from 10 000 to 110 000 nm^2. The accuracy of the contact-area determination for a single particle is principally limited by tip convolution effects; we estimate the corresponding error to be about ±5%, as indicated by the horizontal error bars.

To access the error of P_{tip}, multiple manipulation experiments were performed with selected particles and the statistical spread recorded. From this procedure, a statistical error of 10% for the values obtained on HOPG and of 7% of the ones obtained on MoS$_2$ was determined. To this statistical error, we added a systematic error, which is determined by the step width between the last data point where no particle motion was recorded and the lowest value for recorded motion (the threshold value). This systematic error naturally contributes to the error only toward lower values, explaining
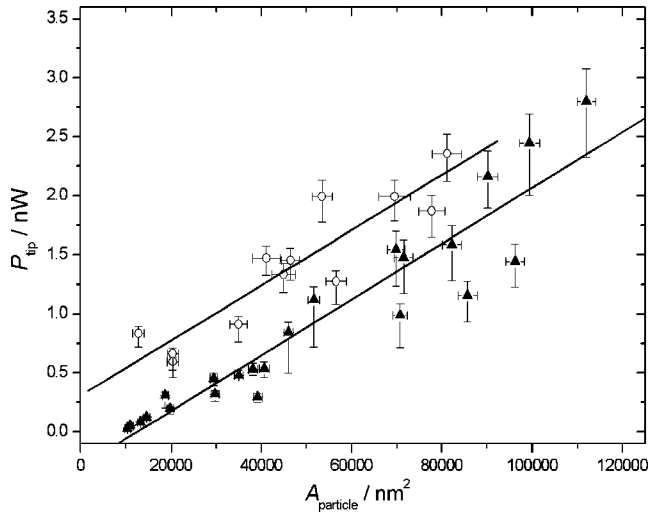
FIG. 4. Plot of the minimum values of power dissipation needed for translation of different-sized Sb nanoparticles on HOPG (filled triangles) and MoS$_2$ (empty circles), respectively. The threshold values for both substrates are in the same range and scale linearly with the contact area of the translated particles. The straight lines represent linear fits of the measured data. The heights of the translated particles were between 21.3 and 28.0 nm with an average value of 26.2 nm for the 23 particles moved on HOPG and between 17.9 and 24.0 nm with an average of 21.5 nm for the 12 particles moved on MoS$_2$.

the significantly larger errors toward lower values than toward larger values featured by certain data points.

The data displayed in Fig. 4 suggest a linear relationship for the dependence of P_{tip} on the particle size $A_{particle}$. For HOPG, we obtain a linear fit of $P_{tip}=(-0.30\pm0.11)$ nW $+A_{particle}\times(2.37\pm0.18)\times10^{-5}$ nW/nm^2, while for MoS$_2$, the corresponding equation is $P_{tip}=(0.31\pm0.17)$ nW $+A_{particle}\times(2.33\pm0.33)\times10^{-5}$ nW/nm^2. Both fit curves are reproduced in Fig. 4.

IV. DISCUSSION

The motivation for our experiments is to study the contact-area dependence of frictional forces in order to shed light on basic mechanisms of friction. Thus, we have to establish a relationship between the dissipation during manipulation (P_{tip}) and the frictional force that a particle experiences while sliding from its start to its end point. This task is anything but trivial, since P_{tip} might be correlated to the static friction force F_s, the height of the energy barrier between two stable equilibrium positions ΔE, or some kind of viscous (i.e., velocity-dependent) damping. Therefore, in parallel to this investigation, an accompanying theoretical study analyzing these issues has been carried out, which will be published elsewhere.[33] However, a simple relationship between P_{tip} and F_s can be established by intuitive ad-hoc arguments, which is corroborated by the more complete treatment presented in Ref. 33.

From the one-dimensional Tomlinson model,[34] we know that a rigid nanoparticle is likely to move from a stable equi-
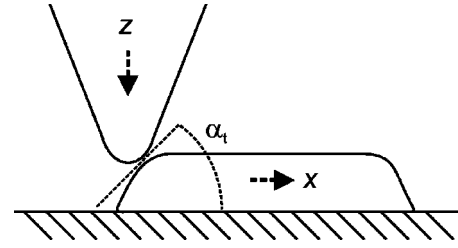
FIG. 5. Sketch of the tip-particle coupling. The impact angle α_t between tip and antimony particle determines the normal (z) and lateral (x) components of the acting force.

librium position to a neighboring one if sufficient energy is provided to overcome the energy barrier between these equilibrium positions. If the distance between these stable equilibrium positions is d, then an upper limit for the minimum energy E_{min} needed to move the particle is $E_{min}=F_s d$. The distance d is of the order of the lattice constant of the substrate, depending on the exact sliding direction relative to the crystal orientation.

On the other hand, P_{tip}/ω is the energy input by the tip per oscillation cycle. At the time when the tip impacts the particle, it receives this energy as kinetic energy $(1/2)mv^2$, where m is the mass of the particle and v its velocity, which has components in both lateral and vertical directions relative to the surface. From Fig. 5, it becomes apparent that only the component in the lateral direction contributes to E_{min}, but not the one in the vertical z direction (which results in elastic deformation). Thus, if the angle between the solid line separating tip and particle in Fig. 5 and the sample surface is denoted as α_t, the component of v in the lateral direction is $v\sin\alpha_t$. Consequently, $E_{min}=(1/2)m(v\sin\alpha_t)^2$ and therefore

$$\frac{P_{tip}}{\omega}=\frac{E_{min}}{\sin^2\alpha_t}\leq\frac{F_s d}{\sin^2\alpha_t}. \qquad (4)$$

From this relation, it follows that $P_{tip}\propto F_s$. A more detailed discussion of these issues can be found in Ref. 33, where we will also argue that the more complete derivation of Eq. (4) leads to an additional factor π in the numerator of the left side of the equation (i.e., $P_{tip}/\omega\approx F_s d/\pi\sin^2\alpha_t$).

Equation (4) enables us to obtain a rough estimate for the shear stress $\tau=F_f/A_{particle}$. Assuming $P_{tip}=0.9$ nW, $\omega=173$ kHz, $\alpha_t=68°$, $d=2.5$ Å, and $A_{particle}=50\,000$ nm^2, which represent typical values for HOPG, we calculate a shear stress of $\tau\leq360$ MPa. We also used $F_f\leq F_s$, emphasizing that τ is defined with the dynamic friction force F_f rather than with the static friction force F_s. Considering the above-mentioned factor π yields $\tau\leq115$ MPa. Slightly higher values are found for MoS$_2$. Even though these values are comparable to values deduced from many friction force microscopy experiments, which are of the order of some hundreds of MPa (cf., e.g., Refs. 5, 8, 12, 15, and 35), they are nevertheless much higher than values for the sliding of complete nanoparticles reported in Refs. 29–31, where shear stresses of 0.1−1 MPa were observed.

The size of the particles translated in Refs. 29–31, however, was of the order of some thousands of nm^2—the par-

ticle sizes studied in this investigation started at about 10 000 nm^2. Interestingly, we see that the energy dissipated during the manipulation of the smallest particles on graphite is very low, and extrapolation of the linear relationship between contact area and dissipated power leads to a negative offset. In fact, we find that nanoparticles with areas below 10 000 nm^2 are so easy to move that it is difficult to quantify the dissipated energy precisely. Even topographic imaging is difficult, since the particles move at already very modest tip-sample interactions [see particle *b* in Figs. 2(c) and 2(d)].

Speculating about the reasons for the observed behavior, let us note that the onset of considerable energy dissipation during manipulation coincides with a structural transformation of the antimony nanoparticles, as it was described in a recent TEM study.[32] There, it was shown that in the early stage of growth small antimony particles with spherical shape and amorphous structure were formed. However, when reaching a maximum diameter of about 110 ± 10 nm, these particles crystallize spontaneously and adopt irregular shapes.[36] Continued deposition leads then to the formation of ramified "flowerlike" particles as shown in Fig. 1. As already discussed in Sec. III A, these particles consist of distinct crystalline domains, which are separated by regions of enhanced stress. Thus, a possible explanation for the observed behavior could be as follows. Particles with areas below about 10 000 nm^2 are amorphous and move as rigid entities, as is required for the occurrence of structural lubricity.[18] Then, the measured shear stress should decrease with the square root of the area,[17] and very low overall values are expected. Presumably, the structural transition taking place at a particle diameter of 110 nm prevents the particles from continuing moving as essentially rigid bodies. Instead, the particles start dislocating in steps, where rigid entities or "domains" cause internal deformations between other "domains" that are not yet moving. This behavior would add an additional route for energy dissipation, which has characteristics similar to the popular Frenkel-Kontorova model of friction[37] (i.e., individual rigid areas are connected by compliant springs that are deformed in the sliding direction and cause elastic multistabilities).

This simple picture would explain two of the main characteristics of the data shown in Fig. 4. First, for a mechanism as outlined above, we would expect a linear relationship between P_{tip} and $A_{contact}$, since larger particles incorporate more areas of enhanced stress that might dissipate energy during manipulation. Second, this picture would also explain why we find roughly the same slope for the $P_{tip} \propto A_{contact}$ dependence on both HOPG and MoS$_2$: With the energy being almost entirely released in the antimony nanoparticles, there is little influence of the substrate on the total energy dissipation. We would nevertheless like to point out that in all experiments, the contact pressure was approximately the same (essentially defined by the acting adhesive forces between particle and substrate). Thus, extrapolations to the case where contact areas change due to an increase or decrease in contact pressure are not possible.

The larger offset of the linear fit for the particles on the MoS$_2$ substrate, however, remains to be understood. Possi-bly, this could be due to an enhanced chemical interaction between the antimony and the sulfur atoms as opposed to the interactions between the antimony and the carbon atoms at the inert HOPG surface. Alternatively, it could be related to the observation by means of TEM and electron diffraction that the antimony nanoparticles grown on MoS$_2$ are strongly textured on the contact side. The crystal orientations are found to be preferentially oriented to the substrate plane rather than distributed randomly. This indicates a structural relationship between the antimony particles and the MoS$_2$ substrate. In contrast, such an effect was not observed for particles grown on HOPG.

To conclude this part, we would like to mention that the data displayed in Fig. 4 represent values for particles that have been moved before. About 30% higher values than the ones reflected in Fig. 4 were found to initiate the dislocation of nanoparticles for the first time. This could indicate that the antimony atoms at the interface rearrange in an unknown manner once the substrate-particle bonds are overcome for the first time, or that the orientation of the particles relative to the substrate changes due to rotation, which reduces the overall interaction strength.

V. CONCLUSION

In summary, we have measured the power dissipation P_{tip} occurring while moving antimony nanoparticles on HOPG and MoS$_2$, respectively, as a function of the particle size. For particles with a substrate-particle contact area $A_{particle}$ between 10 000 and 110 000 nm^2, a linear relation between P_{tip} and $A_{particle}$ has been observed. Within a heuristic model, this result suggests a linear relationship between the frictional force and the particle size. In contrast, particles with contact areas below 10 000 nm^2 were much easier to move compared to their larger counterparts. As a possible explanation for these findings, we suggest that particles with areas below 10 000 nm^2, which are known to be entirely amorphous, move as essentially rigid entities and thus show structural lubricity that leads to low friction. Particles with areas larger than 10 000 nm^2, however, consist of several crystalline domains, which are separated by areas of enhanced stress. These different structural properties could enable the temporary occurrence of elastic deformations within the particles during translation (i.e., such larger particles would *not move as internally rigid entities*, even though they still move in one piece), opening an additional avenue for energy dissipation that depends linearly on the particle size.

*Corresponding author. Electronic address: claudia@chemie.hu-berlin.de

†Present address: Fritz-Haber Institute of the Max Planck Society, D-14159 Berlin, Germany.

‡Present address: Federal Institute of Materials Research and Testing (BAM), D-12200 Berlin, Germany.

[1] *Handbook of Nanotechnology*, edited by B. Bhushan (Springer-Verlag, Berlin, 2004), Part A.

[2] J. Hu, X.-D. Xiao, D. F. Ogletree, and M. Salmeron, Surf. Sci. **327**, 358 (1995).

[3] B. Bhushan and A. V. Kulkarni, Thin Solid Films **278**, 49 (1995).

[4] C. A. J. Putman, M. Igarashi, and R. Kaneko, Appl. Phys. Lett. **66**, 3221 (1995).

[5] R. W. Carpick, N. Agraït, D. F. Ogletree, and M. Salmeron, J. Vac. Sci. Technol. B **14**, 1289 (1996).

[6] R. W. Carpick, N. Agraït, D. F. Ogletree, and M. Salmeron, Langmuir **12**, 3334 (1996).

[7] E. Meyer, R. Lüthi, L. Howald, M. Bammerlin, M. Guggisberg, and H.-J. Güntherodt, J. Vac. Sci. Technol. B **14**, 1285 (1996).

[8] M. A. Lantz, S. J. O'Shea, M. E. Welland, and K. L. Johnson, Phys. Rev. B **55**, 10 776 (1997).

[9] U. D. Schwarz, O. Zwörner, P. Köster, and R. Wiesendanger, Phys. Rev. B **56**, 6987 (1997).

[10] U. D. Schwarz, O. Zwörner, P. Köster, and R. Wiesendanger, Phys. Rev. B **56**, 6997 (1997).

[11] P. B. Merrill and S. S. Perry, Surf. Sci. **418**, 342 (1998).

[12] M. Enachescu, R. J. A. van den Oetelaar, R. W. Carpick, D. F. Ogletree, C. F. J. Flipse, and M. Salmeron, Phys. Rev. Lett. **81**, 1877 (1998).

[13] J. Wang, K. C. Rose, and C. M. Lieber, J. Phys. Chem. B **103**, 8405 (1999).

[14] O. Piétrement, J. L. Beaudoin, and M. Troyon, Tribol. Lett. **7**, 213 (1999).

[15] O. Piétrement and M. Troyon, Langmuir **17**, 6540 (2001).

[16] L. Wenning and M. H. Müser, Europhys. Lett. **54**, 693 (2001).

[17] M. H. Müser, L. Wenning, and M. O. Robbins, Phys. Rev. Lett. **86**, 1295 (2001).

[18] M. H. Müser, Europhys. Lett. **66**, 97 (2004).

[19] K. Shinjo and M. Hirano, Surf. Sci. **283**, 473 (1993).

[20] M. Hirano and K. Shinjo, Phys. Rev. B **41**, 11 837 (1990).

[21] M. H. Müser, Tribol. Lett. **10**, 15 (2001).

[22] J. M. Martin, C. Donnet, Th. Le Mongne, and Th. Epicier, Phys. Rev. B **48**, 10 583 (1993).

[23] M. Hirano, K. Shinjo, R. Kaneko, and Y. Murata, Phys. Rev. Lett. **78**, 1448 (1997).

[24] A. Crossley, E. Kisi, J. W. B. Summers, and S. Myhrs, J. Phys. D **32**, 632 (1999).

[25] M. Dienwiebel, G. S. Verhoeven, N. Pradeep, J. W. M. Frenken, J. A. Heimberg, and H. W. Zandbergen, Phys. Rev. Lett. **92**, 126101 (2004).

[26] M. Heyde, K. Rademann, B. Cappella, M. Geuss, H. Sturm, T. Spangenberg, and H. Niehus, Rev. Sci. Instrum. **72**, 136 (2001).

[27] C. Ritter, M. Heyde, U. D. Schwarz, and K. Rademann, Langmuir **18**, 7798 (2002).

[28] B. Anczykowski, B. Gotsmann, H. Fuchs, J. P. Cleveland, and V. B. Ellings, Appl. Surf. Sci. **140**, 376 (1999).

[29] E. Meyer, R. Overney, D. Brodbeck, L. Howald, R. Lüthi, J. Frommer, and H.-J. Güntherodt, Phys. Rev. Lett. **69**, 1777 (1992).

[30] R. Lüthi, E. Meyer, H. Haefke, L. Howald, W. Gutmannsbauer, and H.-J. Güntherodt, Science **266**, 1979 (1994).

[31] P. E. Sheehan and C. M. Lieber, Science **272**, 1158 (1996).

[32] B. Stegemann, C. Ritter, B. Kaiser, and K. Rademann, J. Phys. Chem. B **108**, 14 292 (2004).

[33] D. A. Aruliah, M. H. Müser, and U. D. Schwarz, following paper, Phys. Rev. B **71**, 085406 (2005).

[34] G. A. Tomlinson, Philos. Mag. **7**, 905 (1929).

[35] R. W. Carpick, D. F. Ogletree, and M. Salmeron, Appl. Phys. Lett. **70**, 1548 (1997).

[36] B. Kaiser, B. Stegemann, H. Kaukel, and K. Rademann, Surf. Sci. **496**, L18 (2002).

[37] Y. I. Frenkel and T. Kontorova, Zh. Eksp. Teor. Fiz. **8**, 1340 (1938).